Battery Internal Temperature Estimation for LiFePO? Battery Based on Impedance Phase Shift under Operating Conditions

Authors:

Jiangong Zhu, Zechang Sun, Xuezhe Wei, Haifeng Dai

Date Submitted: 2019-07-26

Keywords: electric vehicles (EVs), phase shift, impedance, internal temperature estimation, lithium-ion battery

Abstract:

An impedance-based temperature estimation method is investigated considering the electrochemical non-equilibrium with short-term relaxation time for facilitating the vehicular application. Generally, sufficient relaxation time is required for battery electrochemical equilibrium before the impedance measurement. A detailed experiment is performed to investigate the regularity of the battery impedance in short-term relaxation time after switch-off current excitation, which indicates that the impedance can be measured and also has systematical decrement with the relaxation time growth. Based on the discussion of impedance variation in electrochemical perspective, as well as the monotonic relationship between impedance phase shift and battery internal temperature in the electrochemical equilibrium state, an exponential equation that accounts for both measured phase shift and relaxation time is established to correct the measuring deviation caused by electrochemical non-equilibrium. Then, a multivariate linear equation coupled with ambient temperature is derived considering the temperature gradients between the active part and battery surface. Equations stated above are all identified with the embedded thermocouple experimentally. In conclusion, the temperature estimation method can be a valuable alternative for temperature monitoring during cell operating, and serve the functionality as an efficient implementation in battery thermal management system for electric vehicles (EVs) and hybrid electric vehicles (HEVs).

Record Type: Published Article

Submitted To: LAPSE (Living Archive for Process Systems Engineering)

Citation (overall record, always the latest version):	LAPSE:2019.0720
Citation (this specific file, latest version):	LAPSE:2019.0720-1
Citation (this specific file, this version):	LAPSE:2019.0720-1v1

DOI of Published Version: https://doi.org/10.3390/en10010060

energies

MDPI

Article

Battery Internal Temperature Estimation for $LiFePO_4$ Battery Based on Impedance Phase Shift under Operating Conditions

Jiangong Zhu [1,2], Zechang Sun [1,2], Xuezhe Wei [1,2,*] and Haifeng Dai [1,2]

1 Clean Energy Automotive Engineering Center, Tongji University, Shanghai 201804, China; zhujiangong@tongji.edu.cn (J.Z.); sunzechang@tongji.edu.cn (Z.S.); tongjidai@tongji.edu.cn (H.D.)

2 School of Automotive Engineering, Tongji University, Shanghai 201804, China

* Correspondence: weixzh@tongji.edu.cn; Tel.: +86-135-0184-8129

Academic Editor: Hailong Li

Received: 17 November 2016; Accepted: 3 January 2017; Published: 6 January 2017

Abstract: An impedance-based temperature estimation method is investigated considering the electrochemical non-equilibrium with short-term relaxation time for facilitating the vehicular application. Generally, sufficient relaxation time is required for battery electrochemical equilibrium before the impedance measurement. A detailed experiment is performed to investigate the regularity of the battery impedance in short-term relaxation time after switch-off current excitation, which indicates that the impedance can be measured and also has systematical decrement with the relaxation time growth. Based on the discussion of impedance variation in electrochemical perspective, as well as the monotonic relationship between impedance phase shift and battery internal temperature in the electrochemical equilibrium state, an exponential equation that accounts for both measured phase shift and relaxation time is established to correct the measuring deviation caused by electrochemical non-equilibrium. Then, a multivariate linear equation coupled with ambient temperature is derived considering the temperature gradients between the active part and battery surface. Equations stated above are all identified with the embedded thermocouple experimentally. In conclusion, the temperature estimation method can be a valuable alternative for temperature monitoring during cell operating, and serve the functionality as an efficient implementation in battery thermal management system for electric vehicles (EVs) and hybrid electric vehicles (HEVs).

Keywords: lithium-ion battery; internal temperature estimation; impedance; phase shift; electric vehicles (EVs)

1. Introduction

Lithium-ion battery, which has been proven to be the ideal power source for electric vehicles (EVs) and hybrid electric vehicles (HEVs), strikes the best balance between power/energy density and costs for energy storage [1,2]. As safety behaviors and a longer cycle life of the battery demands a narrow temperature range, battery temperature always acts as one of the most essential operating parameters [3]. Surface mounted thermal sensors (thermistors and thermocouples) suffer from heat transfer delay due to the thermal mass of batteries. In consequence of cell thermal non-equilibrium, the internal temperature differs from the external counterpart [4]. It is complicated to directly measure the internal temperature of large format batteries in the vehicular application. An on-line detection of battery internal temperature, which is essential to facilitate operation control, can help improve the accuracy of BMS (battery management system) and the security of the power battery (battery pack). The electrochemical-thermal model [5–8] and electrical-thermal model [9–12] are widely employed to investigate the battery temperature performance during high power extraction. Inserted thermal sensors and thermal imaging are also commonly used in battery thermal research [12–14].

Nowadays, a simple technique to monitor battery internal temperature based on impedance measurement has been proposed [15–20]. Hande [15] provided a technique to estimate the cell internal temperature by measuring the pulse resistance. Srinivasan et al. [16] firstly demonstrated the intrinsic relationship between battery internal temperature and the phase shift obtained from EIS (electrochemical impedance spectroscopy). Schmidt et al. [17] introduced a sensorless temperature measurement method for a 2 Ah pouch cell via the real part of impedance spectroscopy at high frequencies with state of charge (SoC) status unknown and they also studied the influence of temperature gradient on the method by experiments. Richardson and Howey [18] proposed a one-dimensional model, which was validated utilizing internal thermocouple measurement, to estimate the temperature distribution for a 2.3 Ah $LiFePO_4$ cylindrical cell by combined the real and imaginary impedance and battery surface temperature. Further, they extended the estimation using an electrical-thermal model coupled with impedance measurement [19]. Schmidt et al. [17] and Richardson et al. [19] also showed that the estimated temperature inferred from impedance represented the equivalent uniform cell temperature. The impedance phase shift is another important parameter in the EIS test. Our previous work [20] has presented evidence for the existence of the intrinsic relationship between measured impedance phase shift and the internal cell temperature with electrochemical equilibrium, which is seldom influenced by battery degradation for an 8-Ah $LiFePO_4$ battery. Raijmakers et al. [4] also put forward an intercept frequency which was extracted from impedance spectra of a $Li(NCA)O_2$ and a $LiFePO_4$ battery and exclusively related to the internal battery temperature based on EIS. As aforementioned, the impedance-based temperature estimation methods eliminate the requirements of too many hardware temperature sensors and knowledge of the cell thermal properties [4,17–19]. Battery SoC and health often visibly change and several effective estimation strategies considering uncertain driving conditions for EVs and HEVs have been presented [21–26]. Zhang et al. [23] proposed an online battery SoC and SoE (state of energy) estimation method. This method was applied based on the hardware-in-loop setup, where the novel adaptive H infinity filter was proposed to realize the real-time estimation of battery SoC and SoE. The experiment results indicated the high estimation accuracy and strong robustness of the method to the model uncertainty and measurement noise. The impedance-based temperature estimation method reveal that there is a certain frequency which is distinctly dependent on the temperature but does not depend on SoC and battery aging state for the $LiFePO_4$ battery [4,20], which is helpful to implement the impedance-based temperature method from lab to online application in consequence of methods capable of measuring impedance spectra using existing power electronics [27,28].

However, to satisfy the criteria of linearity and time invariance [29,30], the impedance is generally measured at an operating point with a perturbation of a small AC (alternating current) signal and long relaxation time, which hinders the practical application of the impedance-based method when the battery operates under charge and discharge conditions. The interpretation of the measured impedance under operating condition should be systematically investigated, particularly the impedance measurement under short-term relaxation time warrants further investigation for effective estimation.

In our previous study [20], the monotonic relationship between impedance phase shift and battery internal temperature, which is employed as a reference to the temperature estimator for $LiFePO_4$ battery, has been identified in the frequency range of 1–100 Hz with electrochemical equilibrium. Influence of battery SoC and aging are negligible in the selected frequency range. In this paper, we extend on our earlier work by investigating and validating the temperature estimation method with the embedded thermocouple under operating conditions. As shown in the flowchart (Figure 1), the relationship between phase shift and internal temperature is firstly reproduced with temperature homogeneities and artificial temperature gradients under the electrochemical equilibrium state. Regardless of battery internal and surface temperature gradients, the measured impedance phase shift with electrochemical equilibrium corresponds to the cell internal average temperature. Secondly, in order to promote the vehicular application, a detailed experiment is conducted to investigate the regularity of battery

impedance phase shift after charge/discharge current excitations with short relaxation time. It is indicated that the impedance phase shift can also be obtained even under the current excitations. The phase shift descends as the relaxation time increases, which is considered the main contribution of this work to improve the accuracy of the estimation method. An exponential equation that accounts for both measured phase shift and relaxation time is established at 10 Hz tentatively. Furthermore, considering the effect of ambient temperature, a multivariate linear equation is derived and verified experimentally. The predicted internal temperature shows good agreement with the measured internal temperature, which guarantees a more precise assessment of the battery internal temperature.

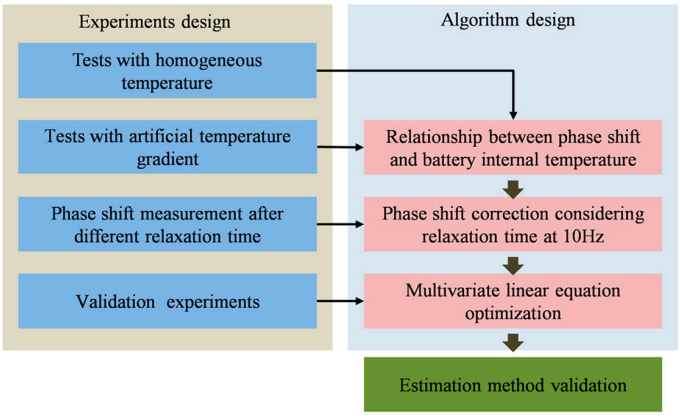

Figure 1. Implementation flowchart.

2. Experiments

The cells adopted in the experiments are commercial $LiFePO_4$ batteries with 30 Ah capacity (Shanghai Aerospace Power Technology, Shanghai, China), as depicted in Figure 2. The specifications of the lithium ion battery used are displayed in Table 1. One thermocouple is placed at the geometric center of the pouch cell in order to directly measure the battery internal temperature. Four experimental procedures are designed as shown in Figure 1, and the detailed introductions are shown in accordance with the orders of their appearance, respectively.

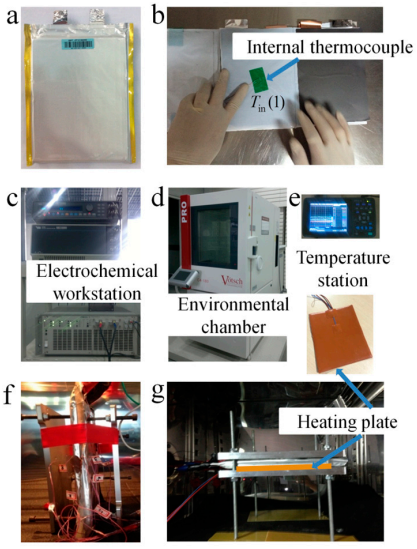

Figure 2. Battery and experimental device. (**a**) The cell sample; (**b**) the location of the internal thermalcouple; (**c**) the electrochemical workstation; (**d**) the environmental chamber; (**e**) the temperature monitor station; and (**f**,**g**) the locations of the cells during tests.

Table 1. Specifications of the lithium ion battery used.

Parameter Name	Values
Nominal voltage	3.2 V
Nominal capacity	30 Ah
Electrode chemistry	$LiFePO_4$/graphite
Internal resistance	$\leq$4 mΩ
Core size	13 mm × 132 mm × 184 mm
Storage temperature	−20–45 °C
Normal Charge voltage	3.7 V
Discharge ending voltage	2.5 V
Weight	0.675 kg
Energy density	144 Wh/kg
Manufacturer	Shanghai Aerospace Power Technology (Shanghai, China)

2.1. Impedance Phase Shift Measurement with Electrochemical Equilibrium

2.1.1. Tests with Homogeneous Temperature

The cell impedance spectra are obtained using an electrochemical workstation (Solartron SI 1287, 1255B, Solartron Mobrey, Durham, UK). The frequency range of the impedance measurement is set to span from 10 kHz to 0.1 Hz with perturbation current of 1.5 A. The ambient temperature is controlled by a Vötsch C4-180 environmental chamber (Vötsch, Germany), as displayed in Figure 2d. Measurements are made over the range −20–40 °C with an interval of 10 °C, and in the range of 0%–100% SoC. The whole test sequence is called A1 for simplification, and the detailed steps are shown in Table 2. The temperatures from all thermocouples are measured utilizing a HIOKI temperature unit (LR8510) (HIOKI, Nagano, Japan) and recorded by a HIOKI wireless logging station (LR8410-30). The tested cell is charged and discharged using an ARBIN instrument (ARBIN, College Station, TX, USA) with the test procedures listed in Table 2.

Table 2. Electrochemical impedance spectroscopy (EIS) test procedures A1 at various state of charge (SoC) and temperature. CC-CV: constant current-constant voltage.

Step No.	Type	Rate	End Condition	Set Temperature (°C)
1	Rest	0	4 h	25
2	Charge (CC-CV)	0.5 C (1 C = 30 A)	Voltage limit 3.7 V; current limit: 0.01 C	
3	Rest	0	2 h	40, 30, 20, 10, 0, −10, and −20 respectively
4	EIS	1.5 A	10 kHz–0.1 Hz	
5	Rest	0	2 h	25
6	Adjust the battery SoC, and repeat the EIS tests			
7	End			

2.1.2. Tests with Artificial Temperature Gradient

To investigate the influence of temperature gradient on EIS measurements, an artificial temperature gradient is constructed. The cell temperature gradients are controlled with the combination of the environmental chamber and a heating plate. Considering the thickness of the cell is 13 mm (Table 1), it facilitates the formation of the stabilized temperature difference, and it is beneficial to verify the relationship between the measured phase shift and the mean temperature value from the results of the embedded thermalcouple, thereby the two lateral surfaces of the cell are imposed [17]. One side of the battery cell is covered with the heat plate, and another side is exposed to the environment as depicted in Figure 3. An internal temperature gradient of the cell forms when

the temperatures of the environment (T_{Am}) and heating plate (T_h) are different. To obtain a more accurate result, two thermocouples are employed to measure the actual temperatures ($T1$ and $T2$) of both side of the cell in each test, and all temperature data are logged as presented in Table 3. $T1$ is the measured surface temperature of the heating plate side, and $T2$ is the measured surface temperature without heating plate. No. 1 represents the uniform temperature of battery which is all involved in the environment chamber without heating plate. No. 2, No. 3, and No. 4 are used to describe the artificial temperature gradient sets. The influence of the internal temperature gradient on battery behavior is investigated at 50% SoC. The particular experiment procedures are illustrated in Table 4.

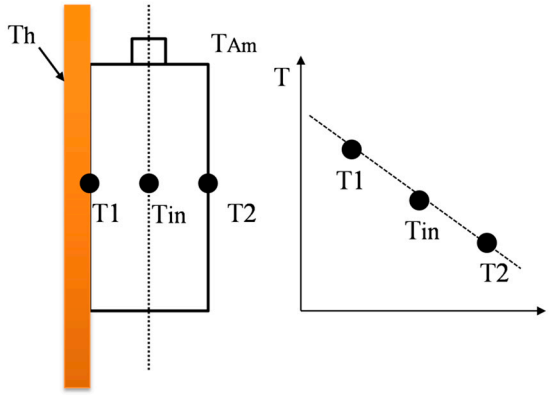

Figure 3. Artificial temperature gradient experiments diagram.

Table 3. The artificial temperature gradients.

Data Sets	*T1*	*T2*	*T1*	*T2*	*T1*	*T2*	*T1*	*T2*	*T1*	*T2*	*T1*	*T2*
No. 1	6		9		12		15		18		22	
No. 2	8	4	12	6	13	11	17	13	21	15	26	18
No. 3	11	1	15	3	16	8	20	10	25	12	29	15
No. 4	14	−3	18	−1	19	5	23	7	28	9	33	11

T1: Surface temperature with heating plate (°C); *T2*: Surface temperature without heating plate (°C).

Table 4. EIS test procedures B1 at artificial temperature gradients at 50% SoC.

Step No.	Type	Rate	End Condition	Set Temperature (°C)	
				Heating Plate	Ambient
1	Rest	0	4 h	-	25
2	Charge (CC-CV)	0.5 C	Voltage limit 3.7 V; current limit: 0.01 C	-	
3	Rest	0	2 h	-	
4	Discharge	0.5	1 h	-	
5	Rest	0	4 h	*T1*	*T2*
6	EIS	1.5 A	10 kHz–0.1 Hz		
7	End				

2.2. Impedance Phase Shift Measurement with Different Relaxation Time

2.2.1. Impedance Phase Shift Measurement after Different Relaxation Time

The experiments are designed to investigate the variation of phase shift after different relaxation time. The whole test sequence is called C1 as depicted in Table 5. The cell is first fully charged by ARBIN at room temperature. The charged cell is discharged to 50% SoC followed by a rest period of

four hours at 20 °C. Then, the cell voltage and temperature are recorded with the 24 A pulse charging and discharging protocol periodically. Subsequently, relaxation time of 0 s, 10 s, 30 s, 60 s, 90 s, and 120 s is set before the EIS experiment, sequentially. After that, four hours rest is scheduled to equilibrate the cell with the chamber temperature again. The temperature control method [31], which leads to a shift of time constants and enlargements of impedance, is a powerful tool in impedance analysis. In order to distinguish each response of elemental steps in the high-medium frequency range, the expansion of impedance measurement are examined by lowering the temperature. Thus, Steps 6–12 are repeated at 10 °C and 5 °C to check the effect of relaxation time on impedance spectrum in more detail.

Table 5. The battery impedance test procedures C1 after different relaxation time.

Step No.	Type	Rate	End Condition	Set Temperature (°C)
1	Rest	0	4 h	25
2	Charge (CC-CV)	0.5 C	Voltage limit 3.7 V; current limit: 0.01 C	
3	Rest	0	2 h	
4	Discharge	0.5 C	1 h	
5	Rest	0	4 h	20, 10, and 5
6	Charge	24 A	10 s	
7	Discharge	24 A	10 s	
8	Repeat Steps 6, 7 200 times			
9	Rest	0	0 s, 10 s, 30 s, 60 s, 90 s, and 120 s respectively	20, 10, and 5
10	EIS	1.5 A	10 kHz–0.1 Hz	
11	Rest	0	4 h	
12	End			

Battery temperature first rises with the increasing pulse cycles and then gradually reaches static state because of thermal equilibrium. Following the pulse experiments described in Table 5, the maximum relaxation period of 120 s is set to ensure that thermal response of the battery to the applied 200 cycles is not obviously altered when the current excitation is switched-off. The cell internal temperature is just dropped by at most 0.3 °C during the relaxation periods monitored by the internal thermalcouple. Therefore, temperature and SoC are assumed to keep constant for all the tests to isolate the effect of relaxation time before EIS tests. The test procedures C2 in Table 6 are designed to obtain the phase shift at the homogeneous temperature with electrochemical equilibrium which refers as the static point in the following discussion. The ambient temperature values inputted in procedures C2 are calculated from battery internal and surface after the period pulse swing in procedure C1 (Table 5).

Table 6. The battery impedance test procedures C2.

Step No.	Type	Rate	End Condition	Set Temperature (°C)
1	Rest	0	4 h	25
2	Charge (CC-CV)	0.5 C	Voltage limit 3.7 V; current limit: 0.01 C	
3	Rest	0	2 h	
4	Discharge	0.5	1 h with 2.5 V	
5	Rest	0	4 h	22 (the temperature after pulse swing)
6	EIS	1.5 A	10 kHz–1 Hz	
10	Repeat Steps 5, 6 two times and Step 5 for 12.5 °C, and 8 °C respectively			
11	End			

2.2.2. Validation Experiments Design

The validation experiments are conducted using constant-current discharge and pulse swing excitation profiles. The procedures of battery charge and discharge are the main factor inducing the variation of battery internal temperature. Based on the above analysis and referring to other research methods for the battery temperature [11,14], the test programs are executed at various ambient temperatures. The discharge pulses of different current magnitudes (15 A, 20 A, and 24 A) are applied to the battery using the TOYO power booster (PBI 250-10) (TOYO Corporation, Tokyo, Japan). The impedance measurements are carried out by 10 s, 30 s and 60 s relaxations with no current load, and the surface and internal temperature are also monitored simultaneously.

3. Results and Discussion

3.1. Impedance Phase Shift with Equilibrium Temperature at 10 Hz

Many studies have elucidated that the EIS characteristics of battery are dramatically impacted by the external environment and internal conditions, especially the temperature [16–20,32]. The electrochemical reaction rate, transfer rate and diffusion rate of lithium-ion are slowed down resulting from the temperature decreasing [32], so the lower temperature enlarges the battery impedance. The EIS procedures A1 are performed and the results are illustrated in Figure 4a. As can be seen, the phase shift changes distinctly with the temperature in the whole frequency range. The relationship between impedance phase shift and battery temperature at 10 Hz is indicated in Figure 4b. A certain frequency range, which is able to exclude the influence of SoC and battery aging on the impedance phase shift, was selected in previous research [4,20]. As illustrated in Figure 4b, the phase shift does not alter with SoC at 10 Hz, which facilitates the impedance-based temperature estimator design since the SoC often visibly changes and is hard to be estimated and calculated in the vehicular application. The phenomenon mainly related to battery electrochemical reaction and diffusion process has been interpreted in our previous study from the electrochemical perspective [20]. In this study, we utilize the phase shift values at 10 Hz tentatively to track the battery internal temperature for the representative of other available frequency points, and the relationship between phase shift and temperature is employed as a reference for the estimation model in the next section.

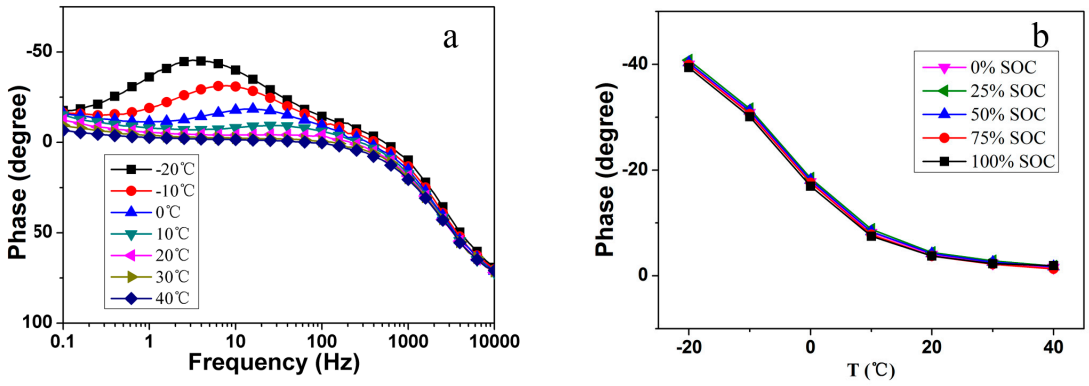

Figure 4. Relationship between impedance phase shift and temperature. (**a**) Phase shift at different frequencies and 50% SoC; and (**b**) the phase shift at various SoC and 10 Hz.

3.2. Impedance Phase Shift with Artificial Temperature Gradients

Some typical EIS measurements at 50% SoC and with different temperature gradients from procedures B1 are depicted in Figure 5. Different temperature gradients are artificially constructed by controlling the temperature of the ambient environment and the heating plate. Because of heat dissipation between cells and the environment, the battery surface temperatures are different with the

setting values, so the actual measured values displayed in Table 3 are used in the paper. The internal temperatures of 6 °C, 9 °C, 12 °C, 18 °C and 22 °C were measured at the central position, and 6 °C (Figure 5a,b) and 18 °C (Figure 5c,d) are presented here for the representative. The black, red and dark cyan color lines represent the battery phase shift measured with thermal equilibrium. The gradient perpendicular to the electrodes is assumed to be linear, as shown in Figure 3. In Figure 5, the impedance spectroscopy and phase shift values are almost the same, even with different temperature gradients, and the effect of high temperature gradients on the phase shift is slightly larger in medium frequencies. It indicates that even under temperature gradients, the cell performs as under a uniform temperature with electrochemical equilibrium. The experimental results are beneficial to the impedance-based estimation method. The effect of temperature non-uniformity on the electrochemical impedance was studied by Schmidt et al. [17], who also proposed that the uniform temperature was the cell internal average temperature based on the impedance results at high frequencies. The variation of the phase shift in our paper may be related to cell impedance characteristics and the experiments schemes. Anticipated detailed interpretation for the measured results will be in next study.

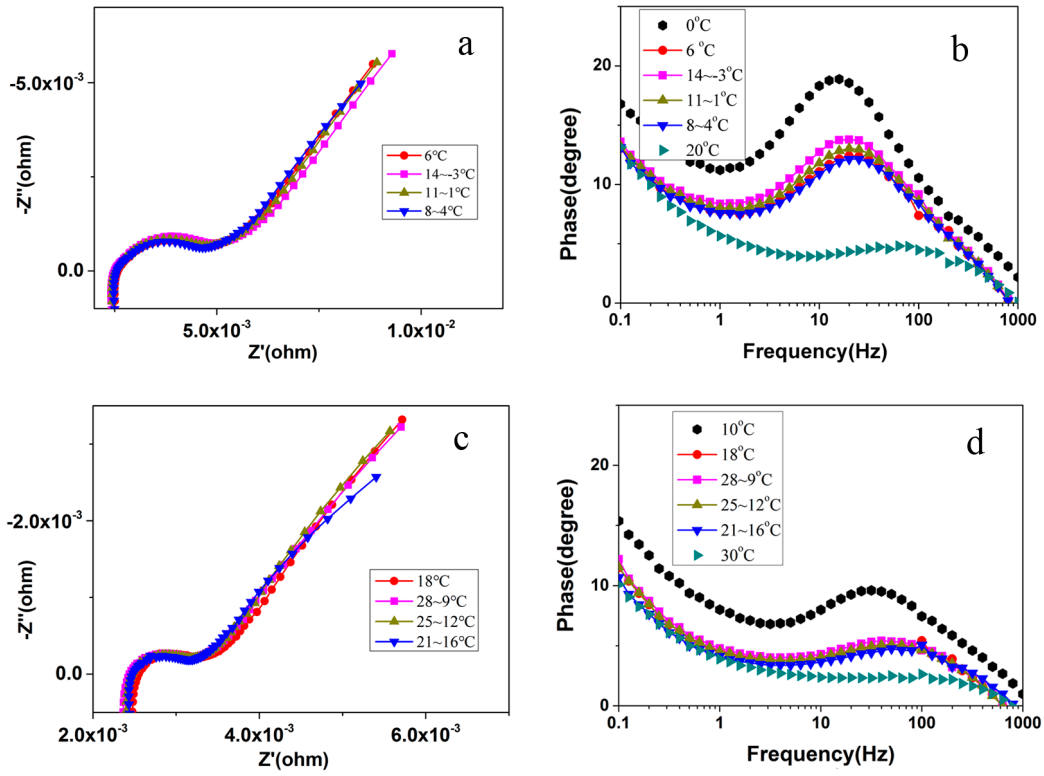

Figure 5. EIS and phase shift with artificial temperature gradients: (**a**,**c**) EIS results; and (**b**,**d**) phase shift results.

3.3. Impedance Phase Shift Correction Considering Relaxation Time

Because of the complexity of the battery charge and discharge process in practical applications, there is seldom sufficient time to satisfy the cell to reach electrochemical equilibrium. The short-term current interruption, such as waiting at red lights, may be the opportunity for AC incentives. Barai et al. [33] and Schindler et al. [34] have studied the impedance of lithium ion cell with different relaxation process between the removal of an electrical load and the impedance measurement. We find that the phase shift is also correlative to relaxation time, especially when the battery is at low temperatures. The impedance measurements are taken after current pulses; when the battery temperature reaches an approximate steady state (200 cycles), the current is switched off to allow the impedance test with different relaxation time.

The evolution of the impedance spectra and phase shift directly after switch-off the pulse current is illustrated for the tests of C1 and C2 in Figure 6. The impedance arc enlarges and the phase shift goes down with the elevation of relaxation time.

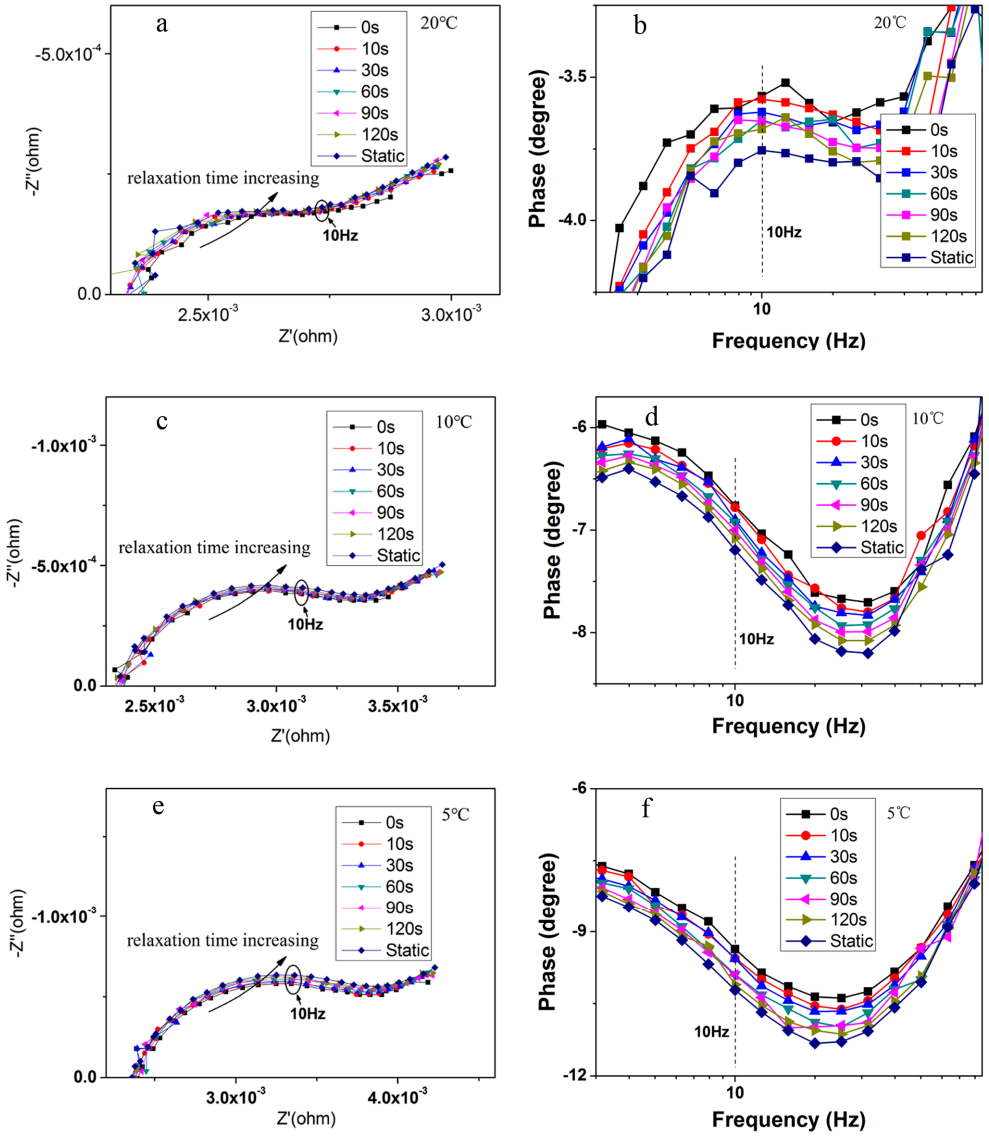

Figure 6. Impedance results at various relaxation time. (**a**) EIS results at 20 °C; (**b**) enlarged phase shift results at 20 °C; (**c**) EIS results at 10 °C; (**d**) enlarged phase shift results at 10 °C; (**e**) EIS results at 5 °C; and (**f**) enlarged phase shift results at 5 °C.

The temperature during the pulse excitation is elucidated in Figure 7. T_{in} is the battery internal temperature, and T_{surf}(1)–(5) represent the battery surface temperature monitored by the thermalcouples. The temperature first ascends with the increment of cycles and then gradually reaches static state due to the thermal equilibrium. The impedance test is performed in the relaxation break as shown the grey rectangle in Figure 7. The cell internal temperature which is monitored by the internal thermalcouple drops by at most 0.3 °C during the maximum relaxation period (120 s). The thermal response of the battery to the applied 200 cycles is not obviously altered when the current excitation is switched-off. It can be argued that the exponential decay of the phase shift is not associated with temperature decay. Therefore, temperature and SoC are kept constant for all the tests to isolate the distraction of relaxation time before cell impedance measurements.

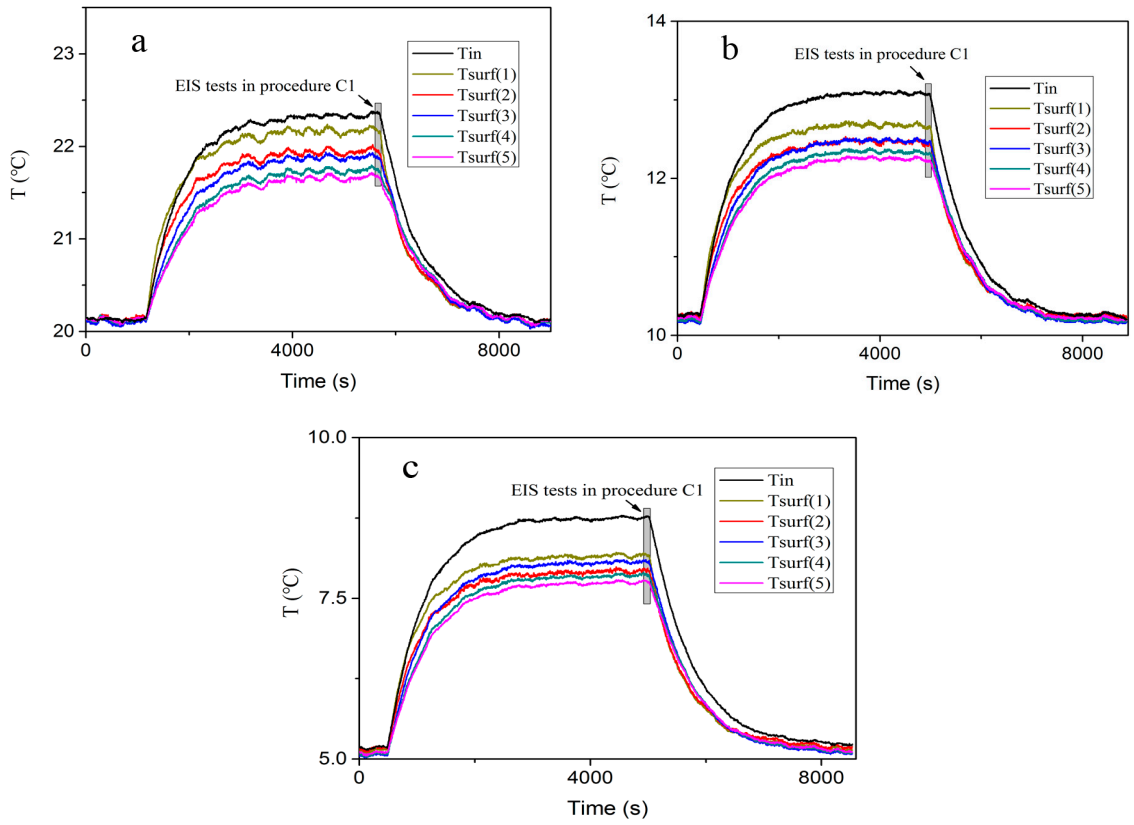

Figure 7. Battery temperatures during the test procedures C1. Battery temperatures at (**a**) 20 °C; (**b**) 10 °C; and (**c**) 5 °C.

The temperature values inputted in procedures C2 is the calculated temperature after the periodic pulse swing, and the impedance obtained in C2 is employed in Figure 6 (static scatters) for comparison. Two major features can be extracted from the results of the recorded spectra: (1) it is apparent that the impedance arc enlarges with the incremental relaxation time gradually, especially at low temperatures; and (2) the phase shift particularly slumps at a certain frequency point. In this study, the phase shift at 10 Hz for the representative of other frequency points is selected to estimate battery internal temperature tentatively, thereby the relationship between phase shift and relaxation time at 10 Hz is displayed in Figure 8. The observed variations are linked to the physical processes occurring at the cell during the relaxation period.

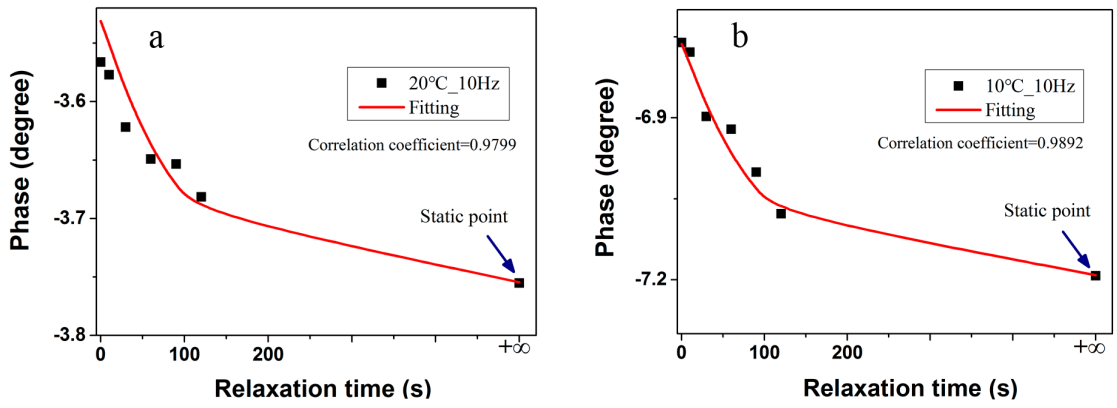

Figure 8. *Cont.*

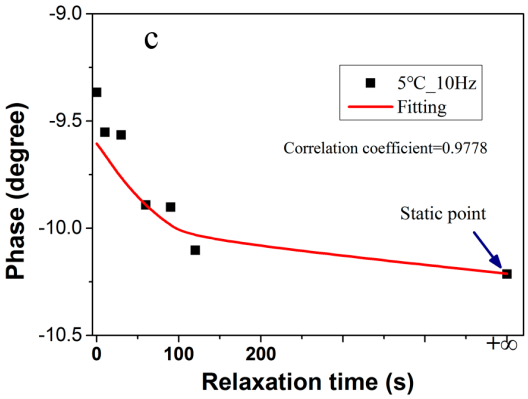

Figure 8. Experimental and fitting results of impedance phase shift at 10 Hz. Phase shift results at (**a**) 20 °C; (**b**) 10 °C; and (**c**) 5 °C.

The EIS is constituted with the impedance under discrete excitation frequency. The phase shift can be obtained from [20]:

$$\varphi(f_x) = \tan^{-1}\left\{\frac{-\mathrm{Im}\{Z(f_x)\}}{\mathrm{Re}\{Z(f_x)\}}\right\},\ x \in [1, 2, \ldots, n] \tag{1}$$

where $f_x, x \in [1, 2, \ldots n]$ is with the variation of excitation frequency.

Battery relaxation is mainly dominated by diffusion processes and may take up to several hours, especially when the battery is almost empty, at low temperature, and after charging or discharging with high current rates [35]. The changes of imaginary part are mainly related to the battery capacitive component. The porosity of the electrodes confers a capacitance to the electrodes when a potential difference is applied to the cell, and the electrodes can be considered as a parallel plate capacitor as described by the Barai et al. [33]. One common observation reports that the capacitance of the cell follows an exponential decay with a subsequent continuous relaxation. The authors attribute their findings to ionic diffusion during the redistribution of ions within the electrolyte after switch-off the pulse current. This redistribution of ions declines the battery capacitance until the overall concentration of the electrolyte reaching equilibrium. As the concentration of ions at the electrolyte surface decreases, when compared to that of the cell under polarization, the total cell capacitance goes down. Therefore, one alternative explanation is that the reduction in the concentration gradients with the electrolyte induces the enlargement of the impedance arc in Figure 6. Because the variation in concentration gradient does not occur instantaneously, but rather occurs at several minutes or hours, the total cell capacitance decreases accordingly as a function of relaxation time. Similarly, the solid state diffusion will occur within the bulk of the particles during the relaxation period, which leads to a rearrangement of the lithium atoms in the electrode materials and will be also reflected in the change of observed impedance arc. S. Schindler et al. [30] also indicated the real part of medium impedance arc rises after the electrical load removed because of battery polarization by experiments.

The shrinking phenomenon of phase shift in Figure 6 should be considered in the temperature estimation method. A possible way to incorporate the information about the relaxation time is to introduce a correction phase shift factor φ', which is calculated from t_{re} and measured phase shift φ, and indicates whether the battery is completely recovered or not. An exponential function corresponding to time is numerously employed to describe the battery relaxation process, such as voltage relaxation [35], and the double layer capacitance relaxation [33]. The phase shift relaxation process is also assumed to proceed as an exponential decay with the time constant τ, and the equation can be described as:

$$\varphi' = \varphi \cdot (1 + \mathrm{a} \cdot \mathrm{e}^{\frac{-t_{\mathrm{re}}}{\tau}}) \tag{2}$$

where a is the pre-exponential factor. We assume that the state of battery does not obviously alert during the frequency sweeping from 10 kHz to 10 Hz, so t_{re} represents the relaxation time, $T_{core} = f(\varphi)$ is the estimated internal temperature with measured phase shift, and $T'_{core} = f(\varphi')$ is the estimated internal temperature corresponding to correction φ'. When a equals 0.065, τ equals 85 s in the equation for the cells, the phase shift of the cell follows the exponential decay, and the experimental data (scatters) and simulation data (line) fit very well as illustrated in Figure 8. Equation (2) takes account for the effect of relaxation time on impedance phase shift, and the evaluation plays a vital role in the subsequent estimation model. In the validation experiments, a relaxation period of 60 s is adopted firstly. The cells are tested utilizing pulse swing excitation profiles above zero temperature, and constant-current discharge at subzero temperature to avoid the lithium dendrites. The temperature of the embedded thermocouple T_{in} is employed to verify the estimated results. The estimated results before and after relaxation time optimization are respectively presented in Table 7. In the results, we can find that the correction Equation (2) can improve the accuracy of the proposed model. The estimated results at a lower temperature are more accurate than that in a higher temperature, which is probably ascribed to the uncertainty of the impedance measurement as the decreasing of impedance at higher temperature. The correction considering the relaxation time, which can promote estimation accuracy, is the main contribution of this work. To further improve the accuracy of the estimator, a multivariate linear regression equation associated with environment temperature is proposed in Section 3.4.

Table 7. The verification of the temperature estimator considering the relaxation time.

T_{Am}	Current	Cycles/SoC	φ	T_{in}	T_{core}	T'_{core}	No.
20 (°C)	24 (A)	500	−2.719	26	27.94	27.42	1
		1000	−2.647	26.3	28.36	27.86	2
	20 (A)	500	−3.074	24.5	25.84	25.26	3
		1000	−3.0548	24.5	25.95	25.37	4
	15 (A)	500	−3.3313	22.5	24.32	23.69	5
		1000	−3.3303	22.7	24.33	23.69	6
10 (°C)	24 (A)	500	−6.983	12.0	12.91	12.37	7
		1000	−7.0134	11.9	12.84	12.29	8
	20 (A)	500	−7.5696	11.1	11.49	10.9	9
		1000	−7.5884	11.0	11.45	10.85	10
	15 (A)	500	−8.0317	10.3	10.37	9.891	11
		1000	−8.0522	10.3	10.30	9.797	12
0 (°C)	24 (A)	SoC I	−9.4269	7.0	8.709	8.395	13
		SoC II	−7.8341	10.2	10.85	10.24	14
	20 (A)	SoC I	−10.331	5.9	7.77	7.426	15
		SoC II	−8.7908	8.6	9.37	9.077	16
	15 (A)	SoC I	−11.294	4.8	6.77	6.393	17
		SoC I	−10.094	6.8	8.016	7.68	18
−10 (°C)	24 (A)	SoC I	−19.94	−2.5	−1.63	−2.12	19
		SoC II	−18.26	−0.5	−0.3438	−0.7924	20
	20 (A)	SoC I	−22.717	−4.7	−3.76	−4.314	21
		SoC II	−17.546	−0.7	0.28	−0.2282	22
	15 (A)	SoC I	−25.138	−6.1	−5.61	−6.227	23
		SoC II	−23.239	−4.9	−4.156	−4.727	24
−20 (°C)	24 (A)	SoC I	−33.087	−13.7	−12.4	−13.57	25
		SoC II	−31.82	−12.5	−11.3	−12.14	26

SoC I represents the 50% SoC; SoC II represents the state of battery reaching cut-off voltage.

3.4. Multivariate Linear Optimization and Validation

The environment temperature, operating time, current and other battery properties all have a great influence on battery internal temperature. Because the impedance reduces significantly at higher temperatures ($T > 10$ °C), a multivariate linear regression equation is established to improve the battery internal temperature estimation accuracy. The relationship is expressed as:

$$T_{\text{mult}} = \beta_0 + \beta_1 \times T'_{\text{core}} + \beta_2 \times T_{\text{Am}} \tag{3}$$

To simplify the algorithm, we assume that the internal average temperature T'_{core} is related to the battery property, and the environment temperature T_{Am} is mainly pertinent to heat dissipation.

When considering the situation in which n independent multivariate observations $x_1, \ldots, x_n$ have been collected, and the number of responses measured in each observation is y, the multivariate linear regression model can be written as:

$$y = \beta_0 + \beta_1 x_1 + \cdots + \beta_n x_n \tag{4}$$

To obtain the parameter vector $(\beta_1, \ldots, \beta_n)$, N sets of observations:

$$X = \begin{bmatrix} x_{11} & x_{12} & \ldots & x_{1n} \\ x_{21} & x_{22} & \ldots & x_{1n} \\ \vdots & \vdots & \ddots & \vdots \\ x_{N1} & x_{N2} & \ldots & x_{Nn} \end{bmatrix}, \; Y = \begin{bmatrix} y_1 \\ y_2 \\ \vdots \\ y_N \end{bmatrix}$$

n is the number of independent variables, N is the number of data sets.

Nine data sets in Table 7 (the even sequences in No. 2–18) are selected to identify the three parameter vector $(\beta_0, \beta_1, \beta_2)$. The goodness of fit ($R$ test), significance test (F test), and regression coefficient significance test (t test) are calculated. The values are all presented in Table 8. At test level $\alpha = 0.05$, all the test values (R, F, and t) prove that Equation (3) is effective and reliable to be used.

Table 8. The parameter vector values in equation.

β_0	β_1	β_2	R Test	F Test		t Test	
				T'_{core}	T_{Am}	T'_{core}	T_{Am}
1.9235	0.7408	0.1829	0.9983	206.5	14.8	10.2	2.7

3.5. Estimation Method Validation

After the obtainment of phase shift according to the correction Equation (1), the measured phase shift can be modified considering relaxation time with Equation (2). Then, the internal average temperature can be calculated from the relationship described in Figure 4. On the basis of multivariate linear equation operation, the estimated temperature T_{mult} can be observed finally.

To further verify the estimated results, a discharge profile is involved at 10 °C and 20 °C as displayed in Figure 9. The AC frequency excitations (10 Hz, dark cyan arrows) are executed after the relaxation process (10 s and 30 s). The estimated temperature results are, respectively, presented in scatters for comparison in Figure 9a,b.

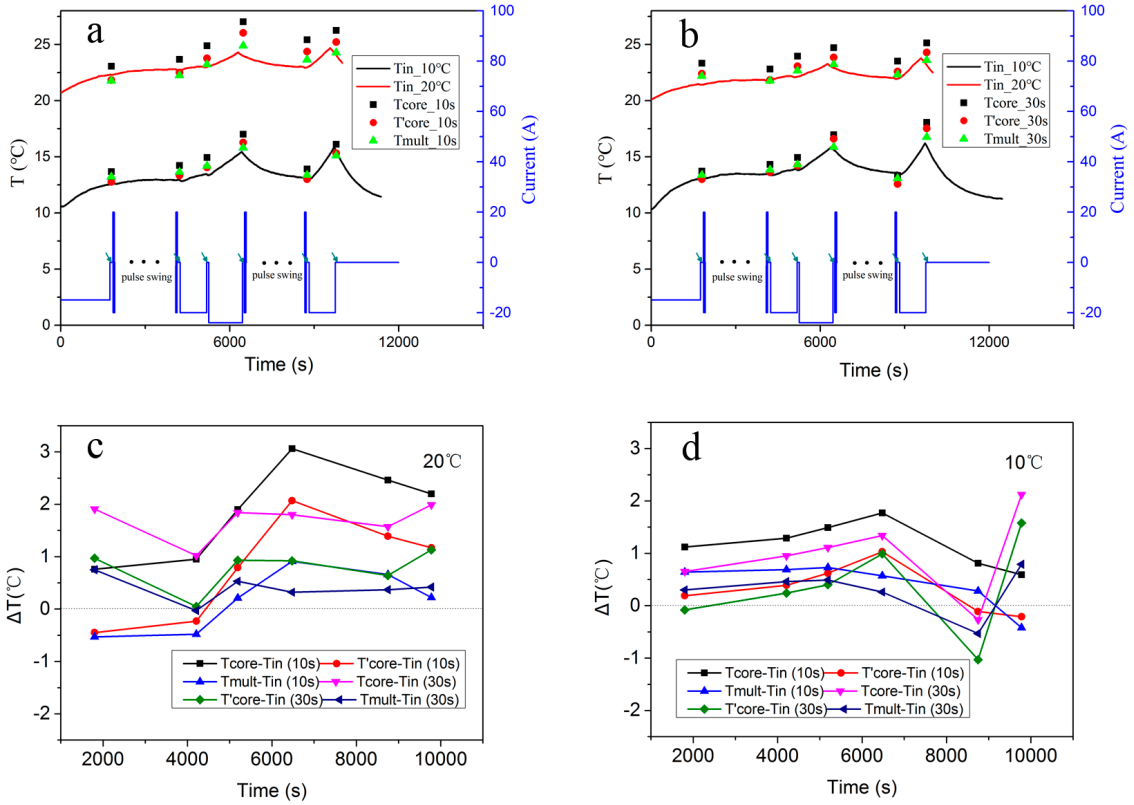

Figure 9. Estimated results with 10 s and 30 s relaxation time. Estimated results with (**a**) 10 s; (**b**) 30 s relaxation time; and temperature error at (**c**) 20 °C; (**d**) 10 °C.

In Figure 9, the estimation temperature T_{core} has larger deviation compared to T_{in}, and the estimation results T'_{core} and T_{mult} show good concordance with the measured cell internal temperature. The results with 30 s relaxation at 20 °C are more accurate than that with 10 s, as shown in Figure 9d. One interpretation is that the battery will be more stabilized and balanced with the incremental relaxation time because of the faster ions transfer and diffusion at higher temperature. Thus, the impedance can be obtained more precisely. Another interpretation could be that the model term to correct for the ambiguous error is more accurate for the 30 s relaxation, as it is already closer to the static value. When the battery operates at 10 °C, the maximum errors are 1.58 °C with Equation (2), and 0.76 °C with Equation (3). When the cells are operated at 20 °C, the errors are 2.07 °C and 0.91 °C, respectively. It indicates that the multivariate linear equation can improve the model accuracy, which mainly contains two aspects: on one hand, Equation (2) is used to modify the measuring deviation caused by electrochemical non-equilibrium. On the other hand, the ambient temperature is introduced in Equation (3) to consider battery temperature distribution due to uneven heat dissipation.

The impedance changes with the degradation of the cell. Identifying ageing and degradation mechanisms in a battery is a main and most challenging goal in the implementation. L.H.J. Raijmakers et al. [4] conduct battery cyclic life tests and their temperature estimated method does not depend on the battery aging. The relationship between the phase shift and battery cyclic aging for the $LiFePO_4$ cell has been discussed in the previous study [20], which shows that the impedance magnitude varies obviously with aging, but the phase shift is not affected by the battery cyclic aging. The aforementioned research facilitates the temperature estimation method in our study. They just test the cyclic life of the cells, however, the calendar life and other complicated utilization mode, e.g., charging and discharging rates like the ones corresponding to the New European Driving Cycle or Urban Dynamometer Driving Schedule, may cause different ageing effects. Hence, validating the relationship between phase shift and other degradation mode is the next focus in our work.

4. Conclusions

Based on the monotonic relationship between impedance phase shift and battery internal temperature proposed in the previous study [20], the impedance-based temperature estimation method is further developed considering electrochemical non-equilibrium caused by current excitation. The impedance phase shift can be measured with a short-term relaxation after the current excitation switch-off. The relationship between phase shift and relaxation time at 10 Hz, which is representative of other frequency points, is investigated tentatively. The results demonstrate that the phase shift descends exponentially with the increment of the relaxation time at 10 Hz, responsible for the redistribution of ions within the electrolyte, which cause the decrease of phase shift after switch-off of the pulse current. An exponential equation is proposed to correct the measuring deviation due to electrochemical non-equilibrium. Considering the temperature inhomogeneities and uncertainty impedance measurement in higher temperature, a multivariate linear equation coupled with ambient temperature is derived. The temperature estimation method may be more accurate in low temperatures corresponding to the high resolution relationship between the temperature and the measured phase shift. The correction proposed in the study is established and verified under the excitation frequency 10 Hz. The model proposed in the paper does not rely on the battery thermal characteristics and surface temperature sensors, it can afford us much convenience in temperature monitoring during cell operating and is also functional as an efficient implementation in battery thermal management system for EVs and HEVs.

Acknowledgments: This work was supported by the National Natural Science Foundation of China (NSFC, Grant No. 51576142), Specialized Research Fund for the Doctoral Program of Higher Education (SRFDP, Grant No. 20130072110055), and International Exchange Program for Graduate Students, Tongji University.

Author Contributions: Jiangong Zhu designed the experiments, analyzed the results and finished the manuscript. Zechang Sun and Xuezhe Wei provided guidance and key suggestions. Haifeng Dai reviewed and revised the manuscript. All authors read and approved the manuscript.

Conflicts of Interest: The authors declare no conflict of interest.

Nomenclature

°C	Degree Centigrade
A	Ampere
C	Current magnitude in terms of cell capacity (1 C = 30 A)
Hz	Hertz
s	Seconds
V	Volt
h	Hour
φ	Measured phase shift
t_{re}	Relaxation time
τ	Time constant
a	Pre-exponential factor
φ'	Correction phase shift factor
t	Time (s)
T	Temperature (°C)
T_{h}	Temperature of heating plate
$T1$	Measured surface temperature of the heating plate side
$T2$	Measured surface temperature without heating plate
Z	Impedance
T_{Am}	Ambient temperature (°C)
T_{core}	Estimated internal temperature with measured phase shift
T'_{core}	Estimated internal temperature corresponding to correction phase shift
T_{in}	Measured internal temperature from embedded thermocouple
T_{mult}	Estimated temperature with Multivariate linear optimization
$(\beta_1, \ldots, \beta_n)$	Parameter vector
f_x	Frequency (Hz)

Acronyms

EV	Electric vehicle
HEV	Hybrid electric vehicle
BMS	Battery management system
EIS	Electrochemical impedance spectroscopy
$LiFePO_4$	Lithium iron phosphate
$Li(NCA)O_2$	Lithium cobalt aluminum nickel oxide
CC-CV	Constant charge-constant voltage
AC	Alternating current
SoC	State of charge
SoE	State of energy

Subscripts/Superscripts

re	Relaxation
h	Heat
Am	Ambient
core	Core
in	Internal
mult	Multivariate

References

1. Takahashi, M.; Tobishima, S.; Takei, K.; Sakurai, Y. Characterization of $LiFePO_4$ as the cathode material for rechargeable lithium batteries. *J. Power Sources* **2001**, *97–98*, 508–511. [CrossRef]
2. Sun, F.; Xiong, R. A novel dual-scale cell state-of-charge estimation approach for series-connected battery pack used in electric vehicles. *J. Power Sources* **2015**, *274*, 582–594. [CrossRef]
3. Yi, J.; Koo, B.; Shin, C.B. Three-dimensional modeling of the thermal behavior of a lithium-ion battery module for hybrid electric vehicle applications. *Energies* **2014**, *7*, 7586–7601. [CrossRef]
4. Raijmakers, L.H.J.; Danilov, D.L.; van Lammeren, J.P.M.; Lammers, M.J.G.; Notten, P.H.L. Sensorless battery temperature measurements based on electrochemical impedance spectroscopy. *J. Power Sources* **2013**, *247*, 539–544. [CrossRef]
5. Wu, B.; Yufit, V.; Marinescu, M.; Offer, G.J.; Martinez-Botas, R.F.; Brandon, N.P. Coupled thermal–electrochemical modelling of uneven heat generation in lithium-ion battery packs. *J. Power Sources* **2013**, *243*, 544–554. [CrossRef]
6. Melcher, A.; Ziebert, C.; Rohde, M.; Seifert, H.J. Modeling and simulation the thermal runaway behavior of cylindrical li-ion cells—Computing of critical parameter. *Energies* **2016**, *9*, 292. [CrossRef]
7. Cai, L.; White, R.E. Mathematical modeling of a lithium ion battery with thermal effects in COMSOL Inc. Multiphysics (MP) software. *J. Power Sources* **2011**, *196*, 5985–5989. [CrossRef]
8. Song, L.; Evans, J.W. Electrochemical-thermal model of lithium polymer batteries. *J. Electrochem. Soc.* **2000**, *147*, 2086–2095. [CrossRef]
9. Capron, O.; Samba, A.; Omar, N.; van Den Bossche, P.; van Mierlo, J. Thermal behaviour investigation of a large and high power lithium iron phosphate cylindrical cell. *Energies* **2015**, *8*, 10017–10042. [CrossRef]
10. Samba, A.; Omar, N.; Gualous, H.; Firouz, Y.; Bossche, P.V.D.; Mierlo, J.V.; Boubekeur, T.I. Development of an advanced two-dimensional thermal model for large size lithium-ion pouch cells. *Electrochim. Acta* **2014**, *117*, 246–254. [CrossRef]
11. Kim, Y.; Mohan, S.; Siegel, J.B.; Stefanopoulou, A.G.; Ding, Y. The estimation of temperature distribution in cylindrical battery cells under unknown cooling conditions. *IEEE Trans. Control Syst. Technol.* **2014**, *22*, 2277–2286.
12. Sun, J.; Wei, G.; Pei, L.; Lu, R.; Song, K.; Wu, C.; Zhu, C. Online internal temperature estimation for lithium-ion batteries based on kalman filter. *Energies* **2015**, *8*, 4400–4415. [CrossRef]
13. Hong, X.; Li, N.; Feng, J.; Kong, Q.; Liu, G. Multi-electrode resistivity probe for investigation of local temperature inside metal shell battery cells via resistivity: Experiments and evaluation of electrical resistance tomography. *Energies* **2015**, *8*, 742–764. [CrossRef]
14. Forgez, C.; Do, D.V.; Friedrich, G.; Morcrette, M.; Delacourt, C. Thermal modeling of a cylindrical $LiFePO_4$/graphite lithium-ion battery. *J. Power Sources* **2010**, *195*, 2961–2968. [CrossRef]

15. Hande, A. Internal battery temperature estimation using series battery resistance measurements during cold temperatures. *J. Power Sources* **2006**, *158*, 1039–1046. [CrossRef]
16. Srinivasan, R.; Carkhuff, B.G.; Butler, M.H.; Baisden, A.C. Instantaneous measurement of the internal temperature in lithium-ion rechargeable cells. *Electrochim. Acta* **2011**, *56*, 6198–6204. [CrossRef]
17. Schmidt, J.P.; Arnold, S.; Loges, A.; Werner, D.; Wetzel, T.; Ivers-Tiffée, E. Measurement of the internal cell temperature via impedance: Evaluation and application of a new method. *J. Power Sources* **2013**, *243*, 110–117. [CrossRef]
18. Richardson, R.R.; Howey, D.A. Sensorless battery internal temperature estimation using a kalman filter with impedance measurement. *IEEE Trans. Sustain. Energy* **2015**, *6*, 1190–1199. [CrossRef]
19. Richardson, R.R.; Ireland, P.T.; Howey, D.A. Battery internal temperature estimation by combined impedance and surface temperature measurement. *J. Power Sources* **2014**, *265*, 254–261. [CrossRef]
20. Zhu, J.G.; Sun, Z.C.; Wei, X.Z.; Dai, H.F. A new lithium-ion battery internal temperature on-line estimate method based on electrochemical impedance spectroscopy measurement. *J. Power Sources* **2014**, *274*, 990–1004. [CrossRef]
21. Sun, F.; Xiong, R.; He, H. Estimation of state-of-charge and state-of-power capability of lithium-ion battery considering varying health conditions. *J. Power Sources* **2014**, *259*, 166–176. [CrossRef]
22. He, H.; Xiong, R.; Fan, J. Evaluation of lithium-ion battery equivalent circuit models for state of charge estimation by an experimental approach. *Energies* **2011**, *4*, 582–598. [CrossRef]
23. Zhang, Y.; Xiong, R.; He, H.; Shen, W. A lithium-ion battery pack state of charge and state of energy estimation algorithms using a hardware-in-the-loop validation. *IEEE Trans. Power Electron.* **2016**. [CrossRef]
24. Sun, F.; Xiong, R.; He, H. A systematic state-of-charge estimation framework for multi-cell battery pack in electric vehicles using bias correction technique. *Appl. Energy* **2016**, *162*, 1399–1409. [CrossRef]
25. Xiong, R.; Sun, F.; Chen, Z.; He, H. A data-driven multi-scale extended Kalman filtering based parameter and state estimation approach of lithium-ion polymer battery in electric vehicles. *Appl. Energy* **2014**, *113*, 463–476. [CrossRef]
26. Xiong, R.; Sun, F.; Gong, X.; Gao, C. A data-driven based adaptive state of charge estimator of lithium-ion polymer battery used in electric vehicles. *Appl. Energy* **2014**, *113*, 1421–1433. [CrossRef]
27. Do, D.V.; Forgez, C.; Benkara, K.E.K.; Friedrich, G. Impedance observer for a Li-ion battery using Kalman filter. *IEEE Trans. Veh. Technol.* **2009**, *58*, 3930–3937.
28. Huang, W.; Qahouq, J.A.A. An online battery impedance measurement method using dc–dc power converter control. *IEEE Trans. Ind. Electron.* **2014**, *61*, 5987–5995. [CrossRef]
29. Mcdonald, J.R. *Impedance Spectroscopy Emphasizing Solid Materials and Systems*; Wiley-Interscience: New York, NY, USA, 1987.
30. Siebert, W.M. *Circuits, Signals, and Systems*; MIT Press: Cambridge, MA, USA; McGraw-Hill Book Company: New York, NY, USA, 1986.
31. Momma, T.; Matsunaga, M.; Mukoyama, D.; Osaka, T. AC impedance analysis of lithium ion battery under temperature control. *J. Power Sources* **2012**, *216*, 304–307. [CrossRef]
32. Zhang, S.S.; Xu, K.; Jow, T.R. Electrochemical impedance study on the low temperature of Li-ion batteries. *Electrochim. Acta* **2004**, *49*, 1057–1061. [CrossRef]
33. Barai, A.; Chouchelamane, G.H.; Guo, Y.; Mcgordon, A.; Jennings, P. A study on the impact of lithium-ion cell relaxation on electrochemical impedance spectroscopy. *J. Power Sources* **2015**, *280*, 74–80. [CrossRef]
34. Schindler, S.; Bauer, M.; Petzl, M.; Danzer, M.A. Voltage relaxation and impedance spectroscopy as in-operando methods for the detection of lithium plating on graphitic anodes in commercial lithium-ion cells. *J. Power Sources* **2016**, *304*, 170–180. [CrossRef]
35. Waag, W.; Fleischer, C.; Sauer, D.U. Critical review of the methods for monitoring of lithium-ion batteries in electric and hybrid vehicles. *J. Power Sources* **2014**, *258*, 321–339. [CrossRef]